UNIVERSITY OF CALIFORNIA,
IRVINE

The Modeling of Pulmonary Particulate Matter Transport Using Langmuir Monolayers

THESIS

submitted in partial satisfaction of the requirements
for the degree of

MASTER OF SCIENCE

in Chemical and Materials Physics – Physics

by

Jeremy M. Eaton

Thesis Committee:
Professor Ilya Krivorotov, Chair
Professor Thorsten Ritz
Professor Zuzanna Siwy

2014

DEDICATION

To my loving parents, John and Joyce Eaton, who instilled in me the sense of discovery that led me to pursue graduate school.

TABLE OF CONTENTS

LIST OF FIGURES

ACKNOWLEDGMENTS

I proudly acknowledge the generous support of the National Science Foundation grant DMR-1309402.

ABSTRACT OF THE DISSERTATION

The Modeling of Pulmonary Particulate Matter Transport Using Langmuir Monolayers

By

Jeremy M. Eaton

Master of Science in Chemical and Materials Physics – Physics

University of California, Irvine, 2014

Professor Ilya Krivorotov, Chair

The effects of a barrier in proximity to the air-water interface on the dynamics of a Langmuir monolayer system are observed. A monolayer of Survanta, bovine lung surfactant, is deposited onto the interface of an aqueous buffer solution. Polystyrene particles one micron in diameter and tagged with fluorescent carboxylate groups are distributed evenly throughout the monolayer surface. The bead-monolayer system is compressed and expanded to induce folding. A polydimethylsiloxane (PDMS) substrate is placed below the monolayer in the buffer solution to study interactions between the folding monolayer and a barrier. The presence of the substrate is shown to shift surface pressure-area isotherms toward regions of lower area by an average of 8.9 mN/m. The surface of the PDMS substrate can be imaged using fluorescence microscopy to detect the presence of particles or surfactant that may have been transported there from the air-water interface during folding. Images show the transferral of particles and monolayer together suggesting the pinch-off of a fold or the direct interaction of a fold with the barrier.

Chapter 1

Introduction

1.1 Biophysics and Soft Condensed Matter

Biophysics is a branch of science that applies principles and theories from physics and physical chemistry in order to understand biological systems. Biophysics is a broad discipline and encompasses everything from using statistical mechanics to model flocking birds [1] to explaining the motion of cellular flagella via energetics and dynamics [2]. Of particular interest is the application of ideas such as complex fluid dynamics and intermolecular dynamics from the study of soft condensed matter to model and explain biological materials.

Soft condensed matter is a branch of materials science which studies matter that deforms easily under the application of an external stress. Stress is a measure of the force per unit area which tends to create deformation within a material. Stress can be applied normal to the surface of a material or in a shear fashion along the plane of the surface. The change in shape due to a stress can be quantified as a strain, which is the amount of deformation some parcel of material has undergone relative to the original shape. Whereas conventional solids exhibit shear stress proportional to the strain, and ideal fluids to the rate at which strain

changes over time, soft matter can display a much wider range of responses and behaviors.

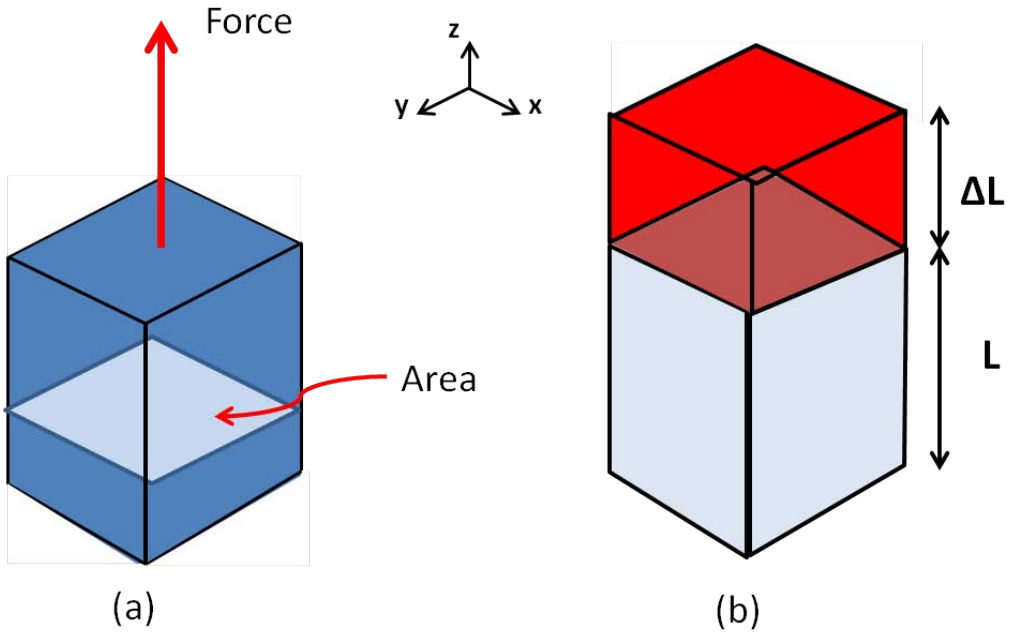

Figure 1.1: Pictorial representations of stress (a) and strain (b). In (a), a force is shown acting perpendicular to the top surface of a block of material. The cross-sectional area this force acts over is highlighted in light blue. In (b), the resulting stress from the force has deformed the material, causing it to elongate in the z-direction. The red portion of the material stretches a length ΔL above the original height of the block (shown in blue), L. The ratio of ΔL to L gives the strain in the material.

One class of soft matter is yield stress materials. These materials possess elastic solid-like behavior until acted on by some threshold stress above which they will flow. Other materials known as "power law fluids" have their shear stress increase as a characteristic power of the applied strain. Viscoelastic materials demonstrate both viscous and elastic responses under deformation. Thus, the relationship between stress and strain for these materials will be time-dependent or by extension, will depend on the frequency at which a periodic stress acts on them. Examples of materials possessing this property include foams, gels and liquid crystals, as well as granular materials such as sand. These classifications are not mutually exclusive. For example, a yield strain material may display a power law relation between the stress and rate of strain once it begins to flow [3].

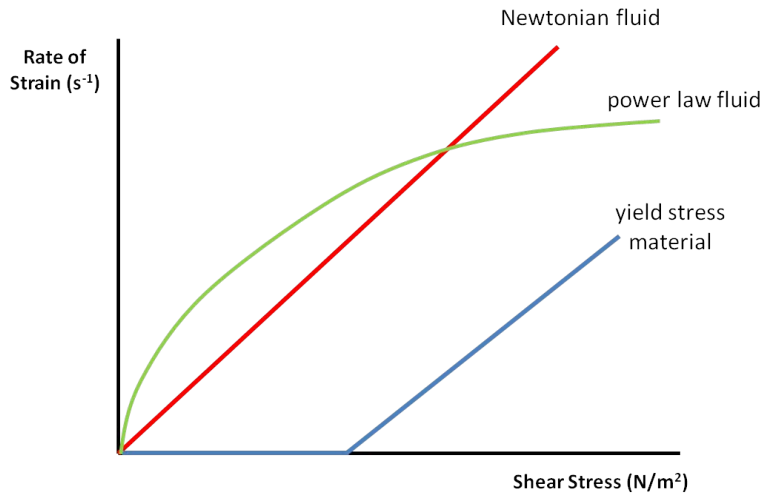

Figure 1.2: Graph showing example relationships between shear stress and the rate of strain for three kinds of fluids. In red is an ideal Newtonian fluid which has a rate of strain that increases linearly with shear stress. The green curve shows the rate of strain for a power law fluid which increases nonlinearly as the shear stress increases. Lastly, in blue, is a yield stress fluid which has zero rate of strain until it begins to flow like a Newtonian fluid above a threshold stress.

Many of the stress-rate of strain relationships for these soft materials have been determined empirically and thus there exists no one overarching theory to explain this wide variety of behavior. Models focusing on the microscopic scale of these fluids have had success explaining some of these behaviors. For example, the rearrangements of adjacent bubbles (T1 events) and the existence of unstable 'weak zones' are posited as some of the driving phenomena that govern a foam's response to applied stress and strain [4]. The mechanisms behind complex fluid behavior for other material remain open questions. For instance, the questions concerning the existence of a yield stress or why the shear stress depends on a particular power of the rate of strain remain largely unanswered.

Materials with negligible thickness (which can thus be approximated as being two dimensional) such as self-assembled monolayers and cell membranes also exhibit viscoelastic properties [5, 6, 7, 8]. These materials display many of the same behaviors seen at the microscopic level in complex bulk fluids and thus their study provides a useful direction in answering the aforementioned open questions. These quasi-2D fluids also have the experimental advantage

of being easy to image by nature of their single plane geometry. Due to these qualities as well as their interesting role in biological systems, the mechanical properties of these quasi-2D materials will be the focus of this thesis.

1.2 Langmuir Monolayers

Nonsoluble amphiphilic molecules will form single molecule thick layers when suspended over an aqueous subphase. This resulting air-water interface is known as a Langmuir monolayer, named after the 1932 Nobel Prize in Chemistry winner, Irving Langmuir. The molecules that form these structures are generally composed of a hydrophilic "head" and a long, hydrophobic "tail". These molecules will align such that their heads are immersed in water while their tails are suspended away from the subphase below. The orientation of these tails will change based on surface pressure in order to minimize the free energy profile of the system [9]. At low surface pressures, the molecules will have their tails arranged in a disorderly fashion with no relationship to one another. As the pressure and thus molecular concentration increases, this so-called "gas phase" gives way to a variety of different phases as the molecules begin to interact with one another [10, 11, 12].

Of most interest to this thesis are the liquid-expanded (LE) and liquid-condensed (LC) phases. The former phase is distinguished by orientation of the hydrophobic tails away from the aqueous subphase, but with no order between individual molecules. As the pressure increases and the area available to each molecule decreases, the liquid-condensed phase begins to dominate and is characterized by an ordered alignment of the molecular tails at some angle above the interface.

In addition to phase transitions, monolayers can also undergo collapse as they are compressed. Here, increased surface pressure in the membrane forces the normally two-dimensional

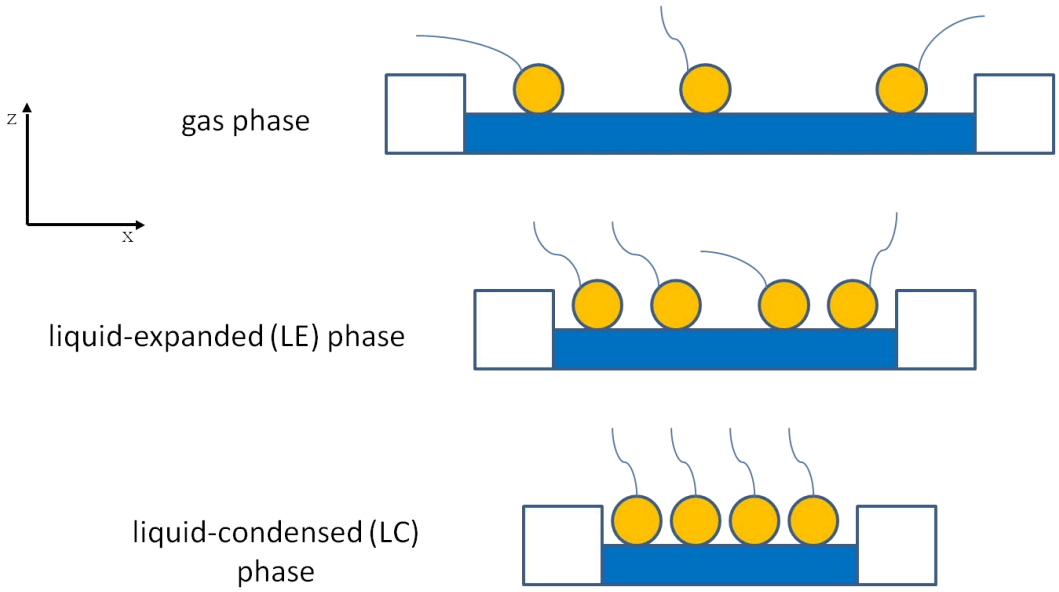

Figure 1.3: Schematic drawings showing the ordering of molecular tails in various phases of a surfactant monolayer between two barriers at the air-water interface. The phases are shown in order of increasing surface pressure from top to bottom. The orange circles represent the hydrophobic heads of the surfactant molecules and the curved blue lines the hydrophilic tails.

monolayer into the third dimension. Conditions for triggering collapse are particular to the material and depend on the rate of compression. These breakdown phenomena include the squeeze-out of material from the interface into small vesicles, buckling and giant folding [13, 14, 15]. The latter type of collapse can have material extrude up to 1 millimeter into the subphase.

Langmuir monolayers are of interest for studying both soft condensed matter and biological physics. Their novel structure makes them ideal experimental subjects for examining complex fluid flow, symmetry breaking [16] and phase transitions under low-dimensional conditions. Monolayers are also present in biological systems. The cell membrane is a lipid bilayer: two monolayers interacting via a weak mutual coupling [17]. The mammalian lung also contains monolayers at air-fluid interfaces in the alveoli which play a vital role in its function. Thus, monolayers are of great interest due to their potential applications in biomechanical and medical fields.

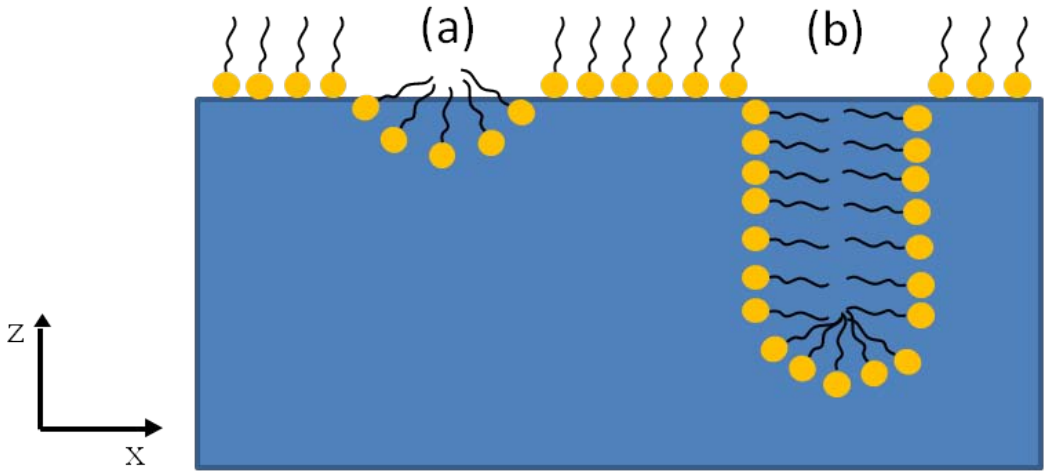

Figure 1.4: Schematic representation of collapse phenomena of a Langmuir monolayer. The left (a) shows a small squeeze-out event and the right (b) shows a large-scale giant fold.

1.3 The Alveolus

Respiration in mammals involves the exchange of carbon dioxide with oxygen gas in the lungs. As air passes down the trachea during breathing, the windpipe branches into many smaller airways known as bronchioles which end in tiny sac-like organs called alveoli. These alveoli provide the surface through which the gases are exchanged to and from the bloodstream. As air inflates them, the surface area through which gas can diffuse increases.

Alveoli are composed of two types of cells: type I and type II. The former variety provide most of the structure of the organ while the latter, larger kind of pneumonocyte is responsible for secreting pulmonary surfactant. This surfactant coats the interior of the alveoli with a monolayer at the interface between the hollow air cavity and the aqueous matter of the epithelial tissue. The monolayer consists of a mixture of proteins interspersed in a matrix of the lipid, dipalmitoylphosphatidylcholine (DPPC). This coating functions as a surfactant to lower the surface tension of this air-fluid interface and therefore decreases the amount of work needed to expand the lung [18, 19] It is also observed that as the lung contracts, the increased surface pressures results in the induction of the liquid-expanded phase in the

monolayer. This increased density is thought to act as a "strut", preventing the lung from completely collapsing during exhalation [20].

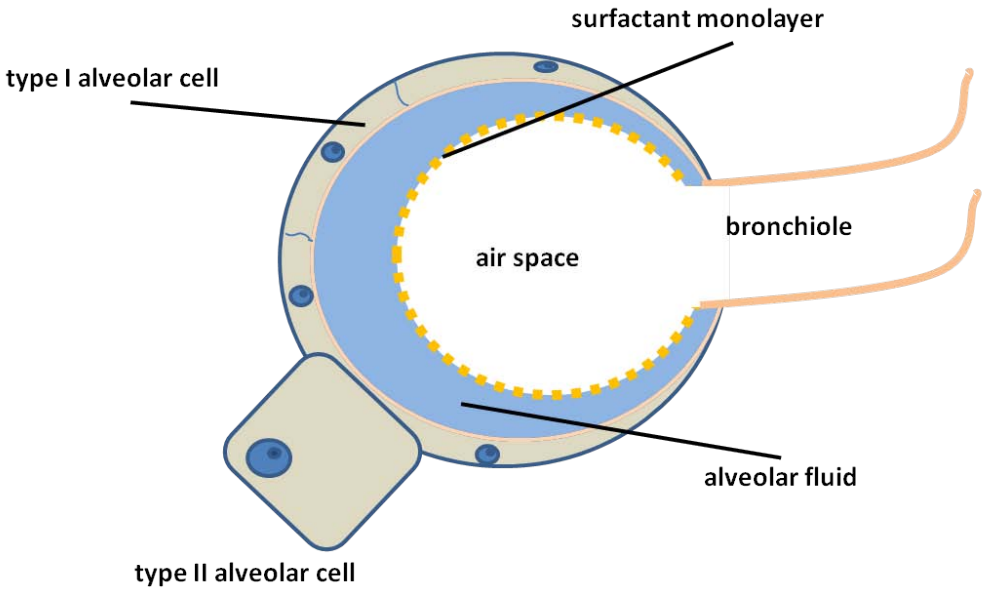

Figure 1.5: Cross-sectional drawing of a single alveolus.

This thesis is concerned with understanding the dynamics of the alveolar surfactant system. Specifically, it will deal with determining methods by which small particles cross the air-fluid interface. In doing so, we explore the not only the interactions of a viscoelastic material with particulate matter, but the potential repercussions that airborne pollutants may have on respiratory health.

1.4 Particle Transport across Monolayers

Atmospheric pollutants and other airborne particulate matter are known to have a negative impact on respiratory health. Particles with a diameter of greater than about 3 microns are swept out of the respiratory system by cilia in the trachea, but smaller particles are able to bypass this defense system and work themselves deeper into the alveolus and ultimately into the bloodstream [21]. It is thus of great interest to determine what mechanisms these particles

are transported across the alveolar surfactant layer and what impact those mechanisms have on pulmonary health.

We propose three primary mechanisms by which particles can transgress the surfactant layer. The first of these involves monolayer collapse into giant folds. Particles deposited into the monolayer may be carried along into these folds and subsequently, the monolayer material may pinch off taking the particles with them. In this mechanism, the particles will be coated as the surfactant will form vesicles around them.

A second mechanism involves particles that have been trapped in folds rupturing through the surfactant leaving the fold to reassemble itself. In this mechanism, the particles can be identified as not being encompassed in a vesicle of the surfactant material.

A third mechanism could occur at the boundaries between regions of different phases. As domains of condensed phase form, they tend to be raised above the region of expanded phases. This uneven topography creates "mesas" between the two phases [22, 23, 24]. It is possible that particles may be able to slip through the spaces formed by these mesas and thus arrive on the other side of the interface. Particles undergoing this transport mechanism should also pass through the surfactant barrier uncoated.

By determining the relative frequencies at which these three mechanisms occur for differing particle sizes, we can then elucidate which airborne particles are most harmful to the lungs or alternatively, find a "safe" particle size that may be ideal for drug delivery using nanoparticles.

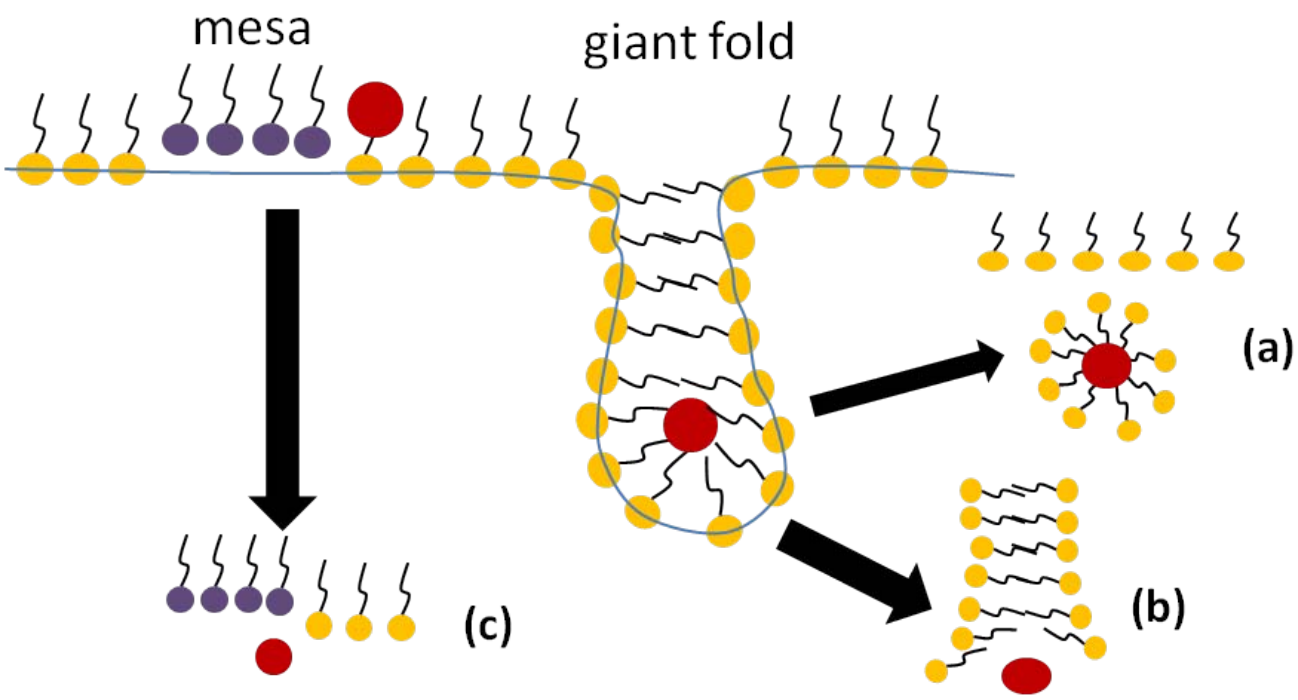

Figure 1.6: Representation of the three mechanisms of particle transport: (a) pinch-off of giant folds, (b) membrane rupture and (c) mesa-based transport at a phase domain boundary. The purple circles represent the hydrophilic heads of a monolayer molecule in the liquid-condensed phase and the yellow are the heads of molecules in the liquid-expanded phase. The red circles represent a spherical particle deposited into the surfactant monolayer.

1.5 Monolayer Dynamics

Although the chemical interactions between particles and the surfactant in the monolayer are suspected to be involved in transport, the dynamical and mechanical properties of the monolayer itself also potentially play a role. For example, monolayers with large bending energy and therefore high stiffness may be less likely to dramatically collapse under compression therefore reducing the relative frequency of pinch-off and rupture transfer methods.

The size of the particles could also play a role in determining its preferred method of transport. If a fold were to form around a larger particle, the higher curvature should increase the stress in the monolayer making it more likely to rupture under additional perturbations. Likewise, very small particles may be ideal for undergoing the mesa-based mechanism of transport due their heightened ability to slip into the openings there. New experimental techniques and tools will need to be developed to dynamically compress and expand the monolayer-particle system while simultaneously assessing the effects of monolayer mechanics and particle size.

1.6 The Key Question

Traditional monolayer experiments are typically performed in a monolayer trough with a depth far larger than the length scales of any collapse phenomena present. As such, the monolayer folds can safely be assumed to interact with only the aqueous subphase below. For the surfactant system in the alveoli, this is not the case. The fluid layer separating the lung surfactant from the alveolar cell line is roughly 0.1 μm in thickness [25]. While we are not able to currently reproduce a gap of that size with reliable precision, we are able to make it significantly smaller than the one millimeter that is transgressed by the largest monolayer folds. Thus, the key question this thesis begins to answer is how the presence of a surface -

such as the alveolar cell line – in close proximity to the air-water interface affects monolayer dynamics as well as transport across the surfactant interface.

It is hypothesized that there will be two kinds of interactions with this surface. The first is a direct interaction in which a collapse structure makes actual contact with the surface. Here, dynamics play a role as the impact may cause the fold to rupture or contort in various ways resulting in pinch-off. Chemical interactions, such as those between the monolayer surfactant and the lipids and proteins in the cell membrane, may also cause the fold to bind to the surface upon contact. The second kind of interaction is indirect in nature. Here, the slip conditions provided by surface may result in new flow patterns in the subphase. These could exert different stresses upon the folds causing them to behave differently than in the large depth limit.

In order to study this system in the context of the lung surfactant, a layer of alveolar cells will be placed in the monolayer trough a short distance below the monolayer. The rest of this thesis will discuss the steps taken to overcome the obstacles in performing such a study. Chapter 2 will provide a survey of the special materials and techniques involved in performing these new experiments. In Chapter 3, I discuss a detailed protocol for culturing alveolar cells for the purposes of use in a monolayer trough. Chapter 4 provides preliminary results for control experiments performed without a "soft" cell boundary, but instead a rigid glass surface. Lastly, Chapter 5 will summarize the observed results from the control experiments and present a framework for future work.

Chapter 2

Experimental Methods

In order to study how the interaction of a monolayer with a surface influences particle transport, several materials and techniques were employed. The first section of this chapter explains the technical details of the lung surfactant monolayer and the particles as well as their roles in the system. The second section explains the major experimental techniques and the associated equipment utilized in this study.

2.1 Materials

2.1.1 Lung Surfactant

Survanta is a bovine lung surfactant purchased from Abbott Pharmaceutical. It is composed of phospholipids, fatty acids and various surface proteins. A neutral buffer solution designed to maintain a pH of 7.4 is made by mixing 2.19g sodium chloride, 0.053g calcium chloride and 0.0082g sodium carbonate per every 250mL of purified Millipore water. The stock solution of Survanta is diluted by the buffer solution in a 1:4 volume ratio. Monolayers of the surfactant

are formed by carefully depositing 150uL of the diluted solution on the surface of an air-buffer solution interface via syringe. Drops of the Survanta are placed evenly over the surface in order to ensure a homogeneous concentration between two Teflon barriers. The system is left for 15 minutes to come to equilibrium before performing any measurements or compressions.

After coming to equilibrium, the monolayer is tagged with 1,2-diphytanoyl-sn-glycero-3-phosphoethanolamine-N-(7-nitro-2-1,3-benzoxadiazol-4-yl) (NBD), a fluorescent lipid very similar in composition to the DPPC in the Survanta. This molecule is added to the monolayer via syringe in a 2 percent ratio to the Survanta already present. NBD absorbs blue light at a wavelength of 460nm and emits back green at 535nm. Adding this tag allows for the selective tracking and highlighting of monolayer-specific features such as folds and phase domains.

2.1.2 Tracer Particles

Spherical polystyrene particles modified with a fluorescent carboxylate group are used as tracers to determine how particulate matter can cross the surfactant boundary. These "FluoroSpheres", purchased from Invitrogen, have an ideal absorption wavelength of 580nm and fluoresce red at 605nm. The particles had a size of one micron in diameter. Before experimental use, the beads were sonicated for 30 minutes to prevent their aggregation. A sample consisting of 100uL of the particle solution is deposited evenly over the monolayer surface using a syringe to ensure a uniform distribution of particles throughout the interface.

2.2 Techiques

2.2.1 Langmuir Trough

The experiments are performed in a Langmuir-Blodgett trough made of Teflon. This basin is filled with 60 mL of the buffer solution so that the fluid has a slight positive curvature above the lip of the trough. The trough is equipped with two motorized barriers also made of Teflon which serve to slowly expand or contract the surface area of the system to a minimum of 20 cm^2 and a maximum of 78 cm^2. The barriers move such that the area available to the monolayer changes at rates ranging from 3 to 134 cm^2/min during both compression and expansion. The temperature of the buffer solution in the basin is held at 37 Celsius by pumping water from a Fischer Scientific Isotemp 1016S into two canals below the basin. This device will also allow us to control the system temperature for temperature dependent experiments in the future.

The trough basin and barriers are thoroughly cleaned before each experiment. First, the barriers are placed at the far ends of the trough. Then, the trough is filled with 18.2 MΩm resistivity water which was dispensed from a Millipore filtration device. The barriers are then manually compressed as to confine any debris or surfactant that may be present. The water is carefully aspirated from the trough and allowed to dry. Next, a small amount of ethanol is poured in the trough and a Kimwipe held in place by forceps is used to swab the surfaces of the trough and barriers. Extra attention should be given to the lens at the bottom of the through as well as the sides and corners of the basin. After about five minutes, the alcohol should be dried and this swabbing process is repeated with chloroform as the solvent. The chloroform evaporates quickly, so there is no need to wait between the next swabbing which is performed with alcohol. After the second alcohol step, the swabbing procedure is repeated one final time with the Millipore water.

This five step cycle can be repeated multiple times if the trough is suspected to be contaminated with excess surfactants or oils. If the trough is especially contaminated, it should be scrubbed thoroughly using detergent under warm flowing tap water for about 15 minutes. Then, this should be repeated with de-ionized water. Once the trough has been sufficiently scrubbed, the five step water-ethanol-chloroform cycles should be performed as normal.

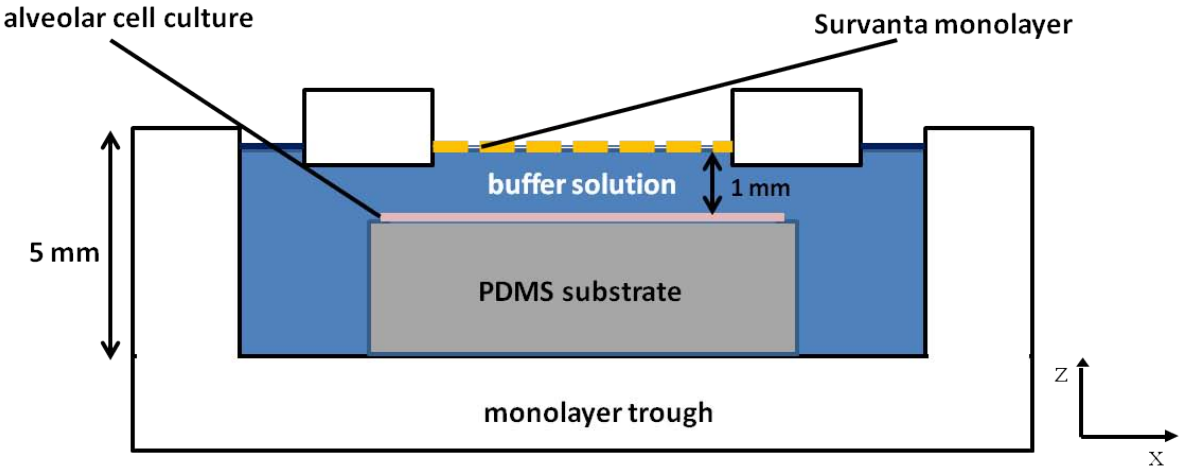

Figure 2.1: Cross-sectional diagram showing the orientation of the components of the monolayer trough viewed from the front.

2.2.2 Fluorescence Microscopy

An Olympus BX60M microscope is used to provide insight on the nature of particle transport across the monolayer of lung surfactant. The microscope is connected to an ORCA-05G digital camera manufactured by Hamamatsu which captures images and videos of the surfactant system and the cell substrate from above. The camera possesses a pixel resolution of 1344 x 1024 and can image at rate of nine frames per second for the purposes of video capture. The microscope is equipped with variable 4x, 10x, 20x and 50x objective lenses which are paired with a 10x magnification eyepiece.

The microscope is equipped with two excitation filters: a wide band blue filter (450-480nm) and a green-yellow filter (535 nm) which are used to induce emission in the tagged monolayer

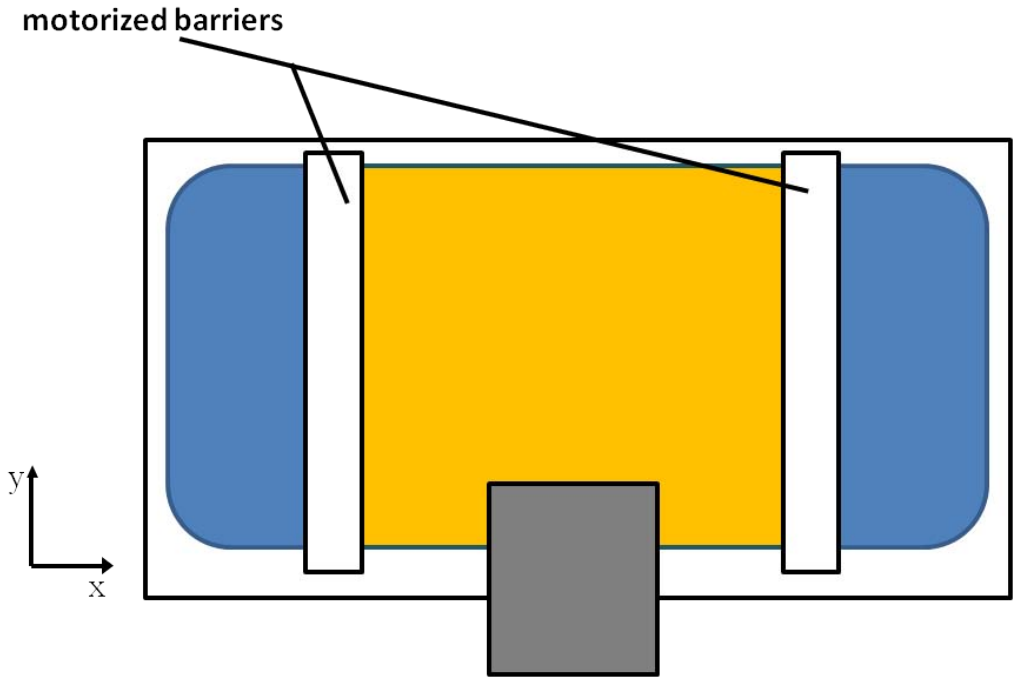

Figure 2.2: Diagram of the monolayer trough viewed from above. The orange region between the barriers shows where the Survanta monolayer will be confined. The gray square at the bottom represents the position of the force transducer from which a Wilhelmy plate will be attached to measure the surface pressure.

and tracer particles respectively. We are thus able to detect a signature wavelength for each of those components. This differential fluorescence allows us to distinctly identify the positions and quantities of both the surfactant and the particles in the captured images and videos.

Videos of monolayer folding and collapse were taken at the center of the trough and viewed under the blue filter. Images of the cell substrate are taken after monolayer collapse and after the subphase is carefully aspirated from the trough. These captures were made at multiple points over the whole of the slide for improved sampling and under both sets of filters.

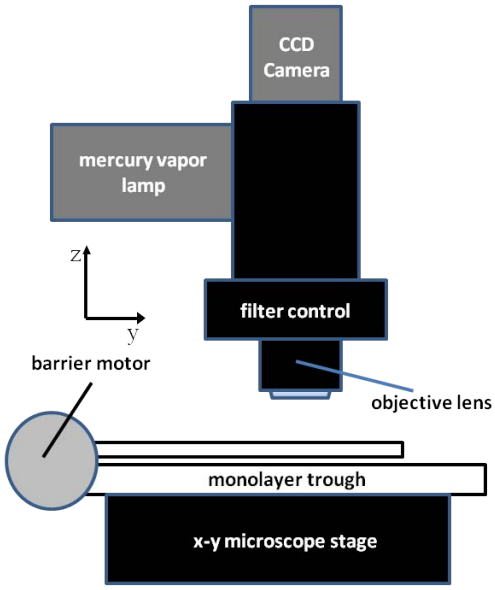

Figure 2.3: Drawing of the complete experimental apparatus featuring the monolayer trough in conjunction with the fluorescence microscope.

2.2.3 Tensiometry

Surface pressure at the air-water interface is measured using a Wilhelmy plate [26]. The "plate" is simply a small paper card measuring one centimeter in the horizontal direction. It is hung from a force transducer and its bottom end is allowed to be submerged in the subphase of the monolayer trough. The forces on the card are the downward force of the card's weight, the buoyant force of the subphase pushing up on the card and the surface

tension at the interface. Zeroing the force transducer after the card has completely soaked up water eliminates the influence of weight and buoyancy and thus the transducer only measures the surface tension forces. The buoyancy does change slightly as water evaporates from the trough leaving less of the card submerged. However, the timescale at which this occurs is much longer than that of the experiment and thus this effect is negligible. These forces can be written as:

$$F_{surf} = 2(w + t)\gamma \cos\theta \tag{2.1}$$

Where γ is the surface tension, w is the width of the card, t is the thickness of the card and θ is the contact angle the surface makes with respect to the plate. The paper card has the advantage of soaking up the subphase which allows the contact angle to go to zero. Assuming a limit where the thickness of the card is much smaller than that of the width, we can thus measure the surface tension at the interface to be:

$$\gamma = \frac{F_{surf}}{2w} \tag{2.2}$$

The measured surface tension can then be converted to the more thermodynamically relevant surface pressure using the following metric:

$$\Pi = \gamma_0 - \gamma \tag{2.3}$$

Where γ_0 is the surface tension of pure water (70 mN/m at body temperature and 72 mN/m at room temperature) and γ is the surface tension of the monolayer system. The constant monitoring of the surface pressure allows for the generation of isotherms which show this pressure as a function of the trough's area. These plots are useful for detecting the occurrence of phase transitions and collapse phenomena as well as tracking the general quality of the deposited monolayer.

Chapter 3

Cell Culturing Procedures

In order to more closely reproduce the conditions present in the lung, a layer of alveolar cells are introduced in the system at a distance of a few hundred microns below the air-water interface. These cells are from the A549 strain and are carcinomic human epithelial alveolar cells first isolated in 1972. In order to raise them near the air-water interface, they are placed on a substrate made of polydimethylsiloxane (PDMS) topped with a 24 x 30mm glass coverslip. By raising the cells toward the air-water interface, the likelihood of an interaction with the collapsed monolayer and the cells is increased. This chapter relates in great detail the steps required to culture and maintain the cell line. In addition, it discusses the challenges of introducing these cells into the trough environment and raising them to level where they are more likely to interact with the monolayer.

3.1 Culturing and Stockpiling Cells

In order to increase the frequency of experiments using the alveolar cell culture, it is useful to grow a large collection of cells that can be stored indefinitely. To do this, one can thaw

out a frozen cell solution in a 37 degrees Celsius water bath. Once thawed, the solution is mixed with 10mL of complete media into a plastic T75 culturing flask. Complete media is a solution composed of the basal media mixed with a 10 percent volume of fetal bovine serum (FBS) and thus contains all of the necessary sugars, proteins and other nutrients the cells need to grow. The flask is then incubated at 37 degrees Celsius for two days. The cells are suitable for removal from the flask surface (known as 'lifting') once they have covered 90 percent or more of the surface.

To lift the cells, the media (now likely a paler red or orange in color) is first aspirated from the flask. The cells are then washed by adding 3mL of Delbecco's Phosphate Buffer Solution to the flask and then rocking the flask gently to rinse the surface. This is done in order to remove excess media and/or debris that may still remain in the flask. This wash cycle is completed by aspirating the buffer solution from the flash. Two more wash cycles are completed using new solution each time to ensure that all of the media is flushed away. Once the flask is sufficiently washed, the cells are still attached to the flask by holdfasts which need to be removed. To accomplish this, 3mL of trypsin, a digestive enzyme, are added to the flask. Once the trypsin is settled uniformly over the flask bottom, the flask is to be incubated at 37 degrees Celsius for two minutes. The cells should be rounded and free-floating in solution at this point. If gently tapping the flask against a hard surface does not dislodge the remaining bound cells, allow an extra two minutes in the incubator. Care is taken not to overexpose the cells to trypsin as they may become damaged or dissolved.

Once the cells are detached, 3mL of new complete media are added to the flask to neutralize the effects of the trypsin. The cell suspension is then transferred to a small vial and is centrifuged at 1000 rpm for 5 minutes. A small pellet of cells should be located at the bottom of the vial. The supernatant above the pellet is aspirated away and remaining cells are then resuspended in 1mL of the culturing medium. The cell pellet is broken up into solution by repeatedly aspirating the mixture with a micropipettor. After the cell solution is

sufficiently mixed, it can be seeded into a new flask for further culturing or onto the surface where they will be used for experimentation.

3.2 Freezing Cells

Alternatively, the cells can be frozen down for indefinite storage. To determine the number of healthy cells that have been grown, the cell density needs to be measured. This is done by first using a micropipettor to place a 10μL sample of the cell suspension into a small centrifuge tube. The suspension is mixed with 10μL of Trypan blue, a dye that stains the cells for easier detection. Ten μL of the mixed sample is transferred to a chamber in a specialized slide which is then placed into a Cell Countess cell counting apparatus. The counter is focused so that the centers of the cells appear bright. Pressing the "COUNT" button on the device gives a readout of the number of cells per milliliter of suspension. The total number of cells present is thus the readout number multiplied by the total volume of suspension solution.

To prepare the cell solution to be frozen, the cell suspension is doled out into specialized cryovials such that there are one million cells in each vial. The cell solution composes eighty percent of the total cryprotectant volume. The remaining volume is composed of 10 percent dimethyl sulfoxide (DMSO), a compound that helps to prevent the cells from bursting as they freeze and 10 percent FBS. Once the solution is well-mixed, the vials are placed in an ethanol bath and frozen at -80 degrees Celsius for at least six hours. The vials should not be left in the freezer for more than two days. Once pre-frozen, the cell samples can be transferred into a liquid nitrogen bath where they can remain preserved for very long time scales.

3.3 Preparing Cells for Experiment

The alveolar cells will be grown not on a flask, but on a glass surface affixed to a PDMS substrate. The substrate is made by mixing a 10:1 mass ratio of Sylgard 184 Elastomer Base to its Curing Agent in a Petri dish. The thickness of the substrate can be modified by utilizing different volumes of the elastomers. The glass coverslip is carefully placed on the surface of the mixture such that the number and size of air bubbles under the slip are minimized. The dish is then baked at 60 degrees Celsius for two hours. Once the mixture is rubbery in texture throughout, the slide is coated with 250μL of a 4:1 solution of Delbecco's Phosphate Buffer Solution and bovine fibronectin protein. After 45 minutes of incubating the protein mixture at room temperature, excess solution is aspirated from the cover slip. The region of the PDMS substrate bearing the coverslip is then excised using a sterile knife. If the cells are cultured on the slip before removing the desired growth region, the probability that some cells will attach to the glass is lowered due to the increased area in which the medium is introduced. The substrate is then placed into a Teflon caddy with a small recess just large enough to allow its easy entry and removal. This ensures that the cell media is only localized to the fibronectin-treated slide. Once fitted into the caddy, the substrate is prepared for cell growth.

The lung cells are first thawed in a warm water bath heated to 37-degrees Celsius. The cell solution is placed in a vial containing 5mL of complete media. The resulting mixture is centrifuged at 1000 rpm for five minutes and then aspirated leaving only a pellet of the cells at the bottom. Once thoroughly mixed into a 1mL media solution, the cells are ready for deposition onto the glass cover slip. The Teflon caddy holding the sample is then placed in a sealed Petri dish and moved to a 37 C incubator where it is left for the cells to grow for two days.

After this time, the cells are transported to the lab and excess media is aspirated from the

Petri dish and the sample is viewed under a microscope to check for confluent growth as well as for any abnormalities. Some cells may die due to cold shock during this transition to room temperature, though the majority will survive if brought back up to temperature within an hour. The substrate supporting the cells is now firmly placed at the center of the monolayer trough such that it should not detach from the bottom surface when the buffer solution is added. Once the trough is full, temperature control should be initiated as soon as possible to minimize the effects of cold shock.

Chapter 4

Data Analysis

Before cells were introduced into the trough, it was necessary to better understand the impact of a physical barrier alone on the collapsing monolayer system. This chapter discusses the procedures and results for preliminary control experiments in which the PDMS substrate was present. In these trials, the substrate was not cultured with a layer of cells, but was topped with a thin glass coverslip. This allows us to compare the results to those from more standard large-depth monolayer experiments and to contrast the effects of a hard boundary with that of the softer one provided by the cells.

4.1 Effect of Decreased Depth – Static

To determine the role of a decreased depth, a PDMS substrate with a thickness of 4mm was fabricated such that the subphase gap between the glass coverslip and the monolayer was less than 1 millimeter. The substrate is placed at the center of the trough and a Survanta monolayer is deposited. As an initial test, the barriers are compressed such that the area is about 50 cm^2 and the system is allowed to sit for a period of one hour. The

Wilhelmy plate monitors the surface pressure as a function of time. A similar experiment was performed without the presence of the PDMS substrate for comparison. Figure 4-1 shows the relationship between surface pressure as a function of time for each of these scenarios.

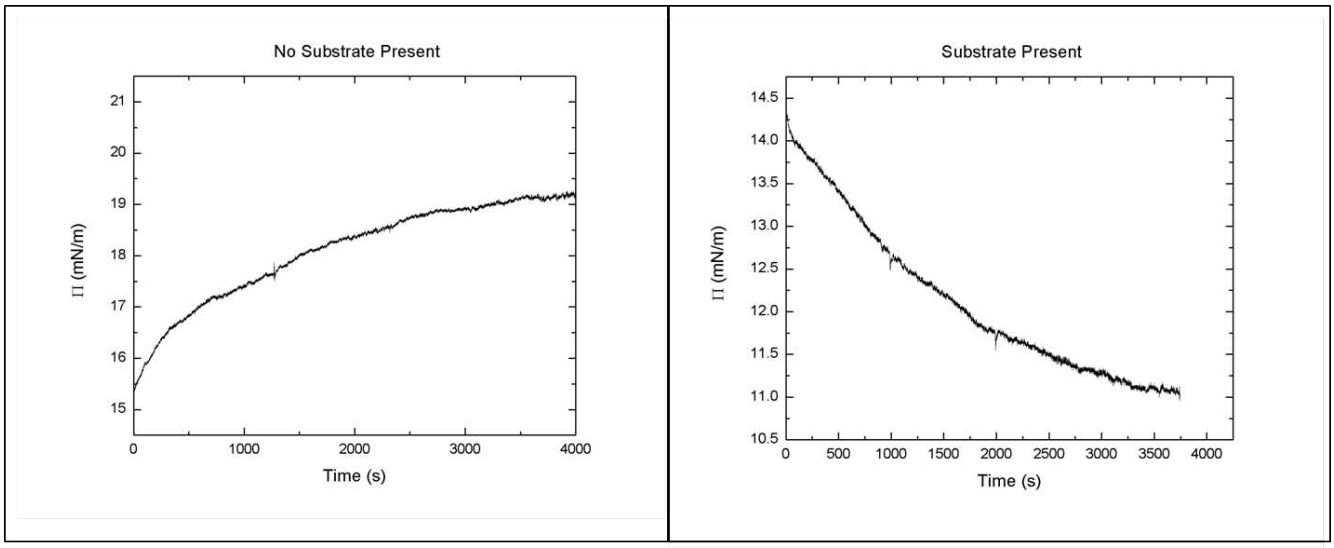

Figure 4.1: Graphs showing the surface pressure vs. time for a Survanta system allowed to sit at an area of 50 cm^2 for a period of one hour. The left graph shows an increase in surface pressure when no substrate is present and a decrease for when the PDMS is placed in the trough.

The experiments show that without the substrate the surface pressure increased by an average value of 4.14 mN/m. This trend is consistent with the gradual evaporation of the subphase. When the monolayer is first deposited, the surface of the subphase has a positive curvature above the rim of the trough. As the water evaporates, the overall depth decreases. This results in a change from positive to negative curvature. The Survanta conforms to this surface and pools at the center of the trough where the Wilhelmy plate is located. The higher concentration of surfactant material in this region results in the higher surface pressure observed.

In contrast, the PDMS substrate showed the opposite effect - the surface pressure decreased by an average of 3.36 mN/m over the course of an hour. This provides preliminary evidence that the reduced-depth geometry of the system significantly changes the nature of the Sur-

factant monolayer. At the low pressure this experiment was performed at, it is not likely that there were direct interactions between the monolayer and the substrate due to the inability to form deep-reaching collapse structures. It is possible that the hydrophobicity of the PDMS may displace water away from the center of the trough. This could direct more surfactant material towards the barriers leaving a larger area per molecule at the center of the trough where the pressure sensor lies.

4.2 Effect of Decreased Depth – Dynamic

In order to determine the effect of reduced depth on the Survanta isotherm cycles, the PDMS was placed in the trough and a series of six complete compression-expansion cycles were performed on a Survanta monolayer. As before, the same experiment was also performed when the substrate was absent. Figure 4-2 shows the differences in the surface pressure as a function of trough area for each case.

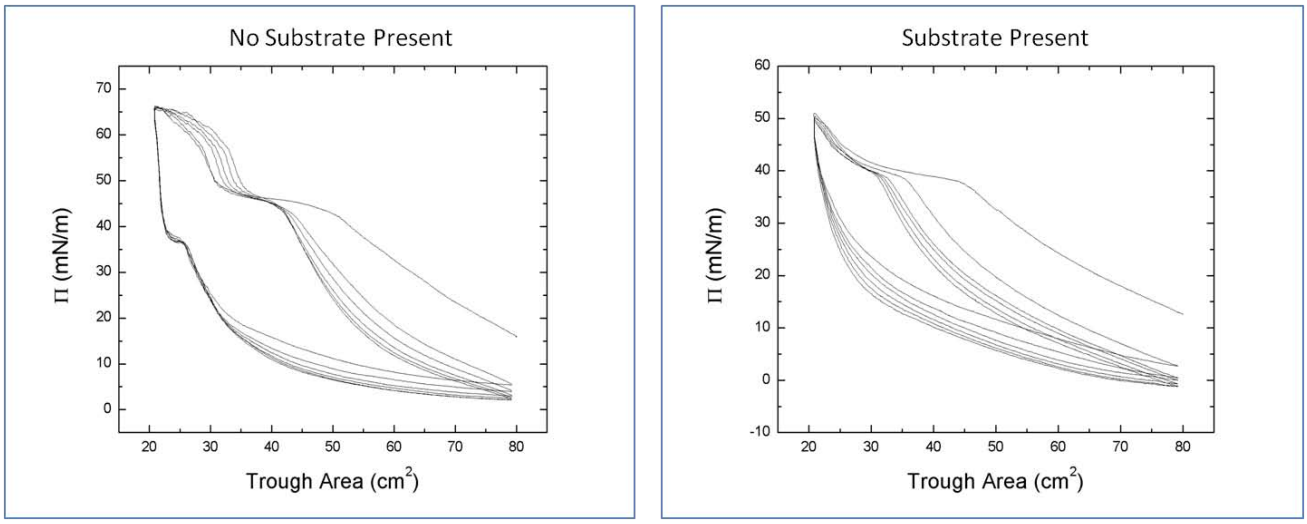

Figure 4.2: Graphs showing the surface pressure as a function of trough area over the course of six full isotherm cycles. The left image shows the case for the large depth limit where no substrate is present and the rightmost graph shows the case for when the PDMS substrate is placed at the bottom of the trough.

Qualitatively, the plots showing the case for large-depth limit have two plateaus: one cor-

responding to squeeze-out at higher area and one corresponding to collapse at smaller area. For the case of the PDMS substrate, the squeeze-out plateau occurs generally at a smaller area than in the large-depth case and the collapse plateau seems to be wholly absent. That is, it appears as if the isotherms shift toward a region of smaller area. Such a shift can arise from a reduced amount of material present at the interface, perhaps lost due to interactions with the substrate below. This is consistent with the observed lower surface pressure at maximum compression for the isotherms with PDMS present than those without. Squeeze-out phenomena generally do not reach sufficient depths to interact directly with the substrate, so the reason for this shift is currently unknown. Theoretical modeling may provide further insight on the exact nature of this transition.

This shift was quantified by first using a custom MATLAB program which works to divide each compression and expansion stroke of the isotherm data into individual pieces. Once each sample of compression data was isolated, they were imported into Wolfram Mathematica. Here, a custom program was designed to determine the initial area where the squeeze-out plateau begins as well as the "width" of this plateau in centimeters squared.

The program begins by taking the difference between surface pressure values in order to obtain information about the local slope for each compression. Due to the pressure sensor's rapid sampling rate, only every fifth data point was used to prevent the presence of false zero slopes. Plotting these slopes as a function of trough area showed that a distinct depression occurred in the region corresponding to the lower rate of change characteristic of the squeeze-out plateau. To determine the initial plateau point, all points below a threshold surface pressure change value of 0.4 mN/m were removed from the data and the difference between adjacent points was calculated. Since no points in the plateau region lie within this data set, the maximum difference found must then correspond to the width of the plateau. The smaller of the two points that make up this difference is lastly recorded as the transition point at which squeeze-out occurs.

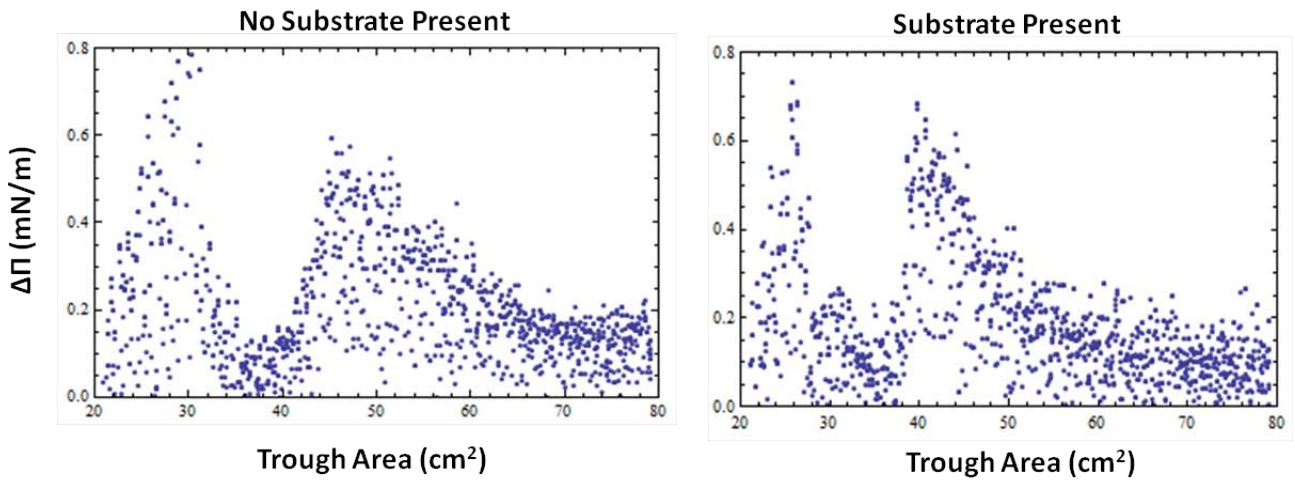

Figure 4.3: Plots showing the change in surface pressure as a function of trough of trough area. The pronounced depression in each graph corresponds to the low rate of change seen in the squeeze-out plateau region of the isotherm compressions.

It is determined that in the presence of the PDMS substrate, the beginning of the squeeze-out plateau is shifted toward lower area by an average amount of 8.9 cm^2. This significant shift indicates that the decreased depth of the system affects the monolayer. Greater interactions between the air-water interface and cell surface below may cause surfactant material to be lost from the surface and therefore lowers the overall surface pressure of the system as the area then available to each molecule increases.

4.3 Evidence of Pinch-off Mechanism of Transfer

A third initial test to determine the impact of the substrate served to directly look at material that may have been transferred from the monolayer onto the substrate. The PDMS cell substrate was placed at the center of the Langmuir trough prior to filling it with the buffer solution. A Survanta monolayer was deposited onto the air-water interface of the trough and particles one micron in diameter were dispersed evenly throughout the monolayer. The system then was equilibrated for an hour with the barriers at their maximum distance apart. After this time, the surface of the substrate was imaged using the fluorescence microscope

and photographs were taken. Images taken at this point using the green filter reveal several particles that have transgressed through the membrane. These particles most likely were forced across the monolayer during the initial deposition process. Under the blue filter, the surface is devoid of any features suggesting that the Survanta has not left the interface.

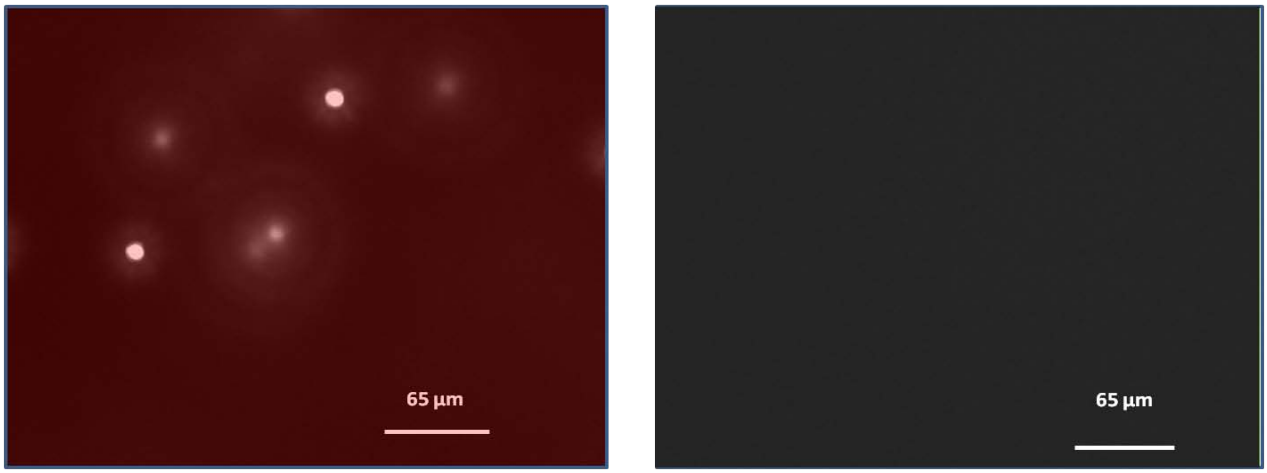

Figure 4.4: : False color images of the PDMS surface taken after 1 hour after depositing particles on to the Survanta monolayer surface. The left image (colored red) shows a few particles deposited onto the substrate with several others (shown out-of-focus) floating above in the subphase. The right image shows the same spot viewed under the Survanta filter. No features can be seen in this view.

After sampling a sufficient area of the substrate for deposited particles and surfactant, the Survanta monolayer is carefully aspirated from the surface and then the bulk subphase is likewise removed. This allows the surveying of the substrate surface for deposited particles and surfactants without introducing any unwanted currents or fluid motion. While aspirating, care is taken so that the monolayer directly above the substrate is removed first. This prevents large rafts of surfactant from depositing themselves onto the substrate, thus obscuring any particles or surfactant structure. Figure 4-5 shows a region of the substrate that has been coated this way in surfactant material. Such regions should be excluded from analysis.

Once the surfactant and subphase are removed, particles and surfactant material that had crossed the monolayer boundary now come to rest on the substrate. Figure 4-6 shows this dry

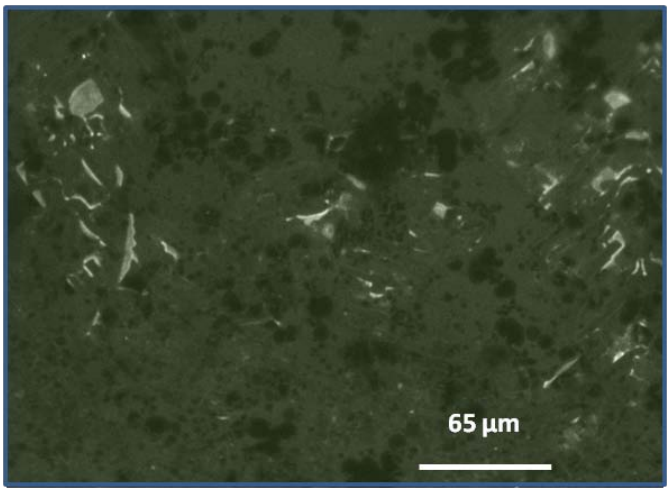

Figure 4.5: False color image of a monolayer raft deposited onto the surface of the PDMS substrate under the blue filter. These rafts obscure transported particles or pinched-off surfactant and thus careful aspiration should be performed to prevent their formation.

surface under both the green and blue filters. It is observed that more particles are apparent than in the previous image due to them coming from the subphase. It is also seen that like in the pre-aspirated image, there is no significant amount of surfactant. This suggests that very little surfactant and few particles are transported across a monolayer without some sort of dynamic mechanism. This supports the hypothesis that transport is mediated via the folding and/or phase separation that occurs as the monolayer compresses and expands. This experiment also acts as the primary control with which images taken after isotherm cycles will be compared.

To determine the effect of dynamic compression and expression of the monolayer on transport, the monolayer-particle is system is allowed to sit for an hour as before. However, instead of vacuuming away the subphase at this point, the monolayer is compressed to an area of 20 cm^2 at an areal speed of 15 cm^2/min. Ten complete cycles of expansion and compression are formed. After the completion of the final cycle, the monolayer and subphase are aspirated away as before. As shown in Figure 4-7, the PDMS subphase now displays the presence of structures under both the particle and surfactant specific filters. The green filter shows particles distributed in a non-random fashion, while the blue filter shows long strands

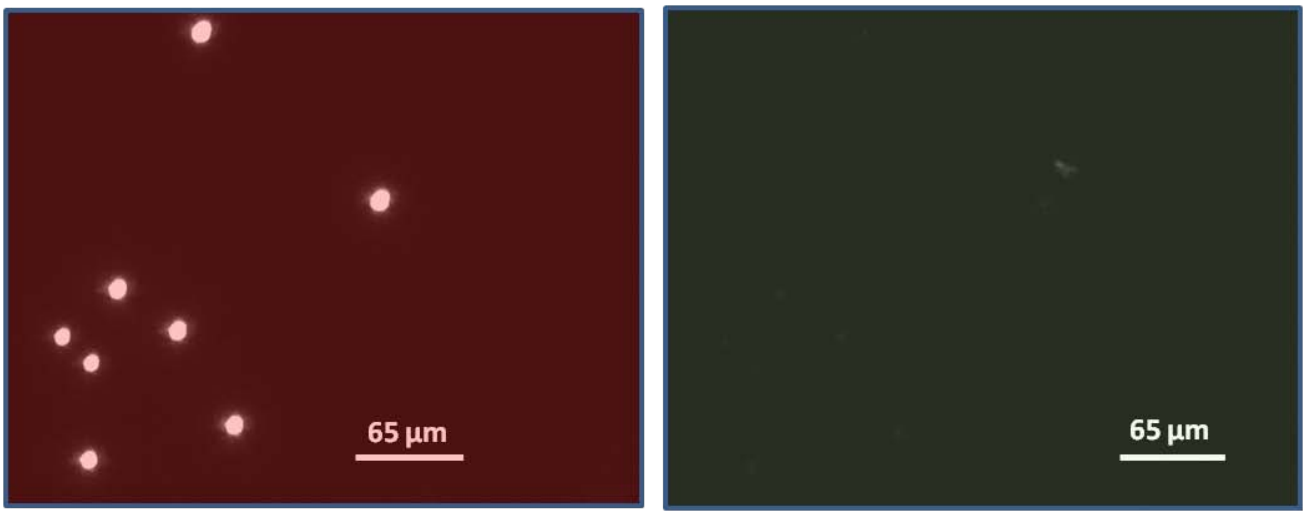

Figure 4.6: False color images of the PDMS surface after aspirating away the subphase and Survanta monolayer. The left image is viewed under the green filter and shows a number of particles that have crossed the air-water interface. The right image is viewed under the blue filter and shows that only a few small agglomerations of Survanta have left the monolayer plane.

of surfactant material arranged in the same pattern as the particles. This implies that the surfactant has wrapped around the particles in a tube-like structure. Such a structure could be formed as a giant fold containing beads is pinched or brushed off from the rest of the monolayer. This structure can then be buffeted by perturbing forces in the subphase causing it to twist and cross-over itself until it is deposited down onto the substrate below. Thus, the appearance of the particles and the surfactant forming the same structure provides evidence that the pinch-off mechanism for transport may occur for particles one micron in size. There is also the strong possibility that the beads and surfactant were transferred to the substrate during a direct contact with a fold.

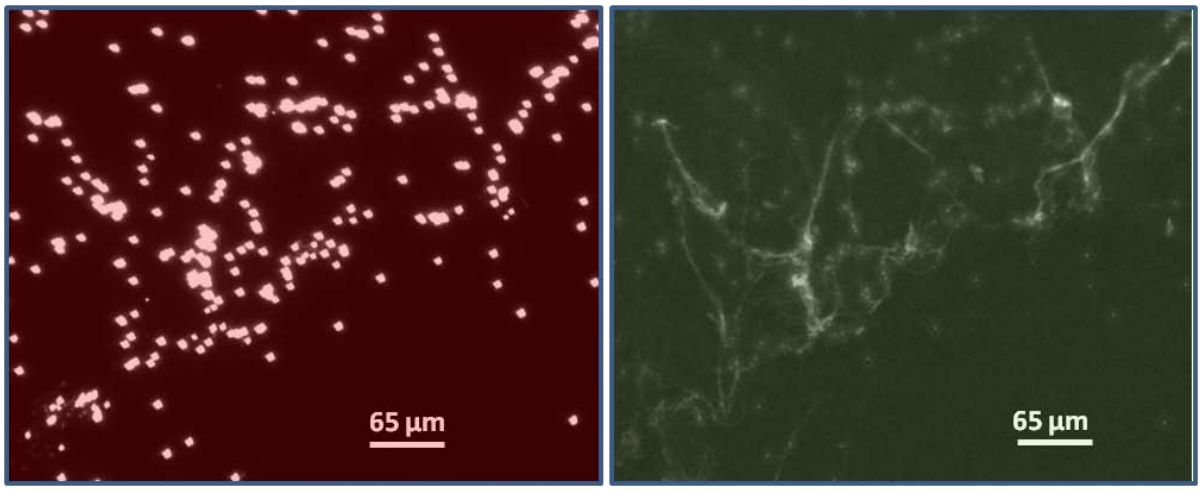

Figure 4.7: False color images of the PDMS surface after perform 10 isotherm cycles and then aspirating away the subphase and Survanta monolayer. The left image viewed under the green filter shows a "constellation" of particles arranged in a structured, non-random fashion. The right image viewed under the blue filter shows a weblike network of surfactant in the same pattern as the particles.

Chapter 5

Conclusions and Future Work

5.1 Conclusions

These studies provide a preliminary look at the nature of how particulate matter is able to be transported across a surfactant monolayer. It is observed that transport is not primarily a result of passive diffusion and that dynamic processes are required. Through these processes, phase separation and collapse can occur which provide mechanisms for the particles to arrive across the boundary. It is also seen directly through fluorescence microscopy that particles can be transported by being encompassed into a large fold or other collapse structure and are transported with the fold as it detaches from the rest of the monolayer.

Furthermore, we have preliminary results of the impact of subphase depth on monolayer dynamics. As the depth of the subphase decreases, the collapsing monolayer is more readily able to interact with the surfaces below. Surfactant material can be deposited onto this surface and the surface pressure of the monolayer relaxes. This causes an overall shift of the surface pressure-area isotherm toward smaller area. In contrast to most traditional monolayer experiments which use a very large depth, these studies provide some preliminary insight

on the conditions present in the lung surfactant system where the alveolar fluid subphase is very tenuous.

5.2 Future Experimental Variations

The above experiments provide a preliminary proof of concept for studying the transport of particulate matter across a monolayer interface. Since particles smaller than 3 microns are able to actively penetrate into the alveoli from the atmosphere, it is of great interest to observe how particles smaller than 1 micron affect and move across the lung surfactant. By examining particles 20nm and 500nm in diameter in addition to the micron particles, we are able to better understand the potential health effects due to the full range of particle sizes present in the atmosphere. In addition, changing the speed at which the barriers compress and expand the barriers will be of interest. Children tend to have higher rates of breathing than adults [27] and thus by exploring how transport changes as a function of compression frequency and amplitude can help to understand whether health risks are higher for younger people. Furthermore, the same frequency results could help to identify if a person would be at higher risk for respiratory damage after periods of intense exercise.

In addition to elucidating the frequency and particle size effects on particle transport, it will also be important to understand the effect of depth. It was already observed that effectively decreasing the depth of the trough resulted in a shift of the squeeze-out plateau toward lower area. Future work will vary the depth by creating PDMS substrates of various thickness to model the shift in area as a function of the spacing between the monolayer and the surface below. In doing so, we are able to better understand how these changing boundary conditions affect the hydrodynamics of the system.

The previous experiments are able to find clear evidence of pinch-off transport due to the

"smoking gun" of coating the particles in surfactant. The other mechanisms: rupture and mesa-transport have the particles come through uncoated and thus are indistinguishable using the above methods. To determine the prevalence of mesa-based transport, the monolayer could be compressed to a pressure characterized by the presence of liquid-condensed domains. Particles near the boundaries of these domains could be observed and their number tracked over time. This study would reveal information about the timescales for which mesa-based transport occurs. Thus, this rate could be used to determine what fraction of uncoated particles result from mesa-based transport as opposed to rupture.

As the apparatus currently stands, the cell-bearing substrate remains static below the air-water interface. In order to continue towards more genuinely reproducing the conditions found in the alveoli, the system should be redesigned as to permit the cells to expand along with the monolayer. To accomplish this, they would need to be cultured directly onto a plasma-treated sample of a soft elastic material. Custom modular barriers would be constructed to fit together and to hold the cell culture sample between them. Then, as the barriers expand and contract, the cells are able to behave in the same manner, just as it occurs in the living, breathing lung.

5.3 Supplementary Techniques

There are several techniques that could be added to or performed in conjunction with the current apparatus to provide further insight about particle transport in the surfactant system. Ellipsometry is an optical technique that measures the polarization of reflected light in order to measure thin films. This would be applied to measure more accurately the depth of the subphase gap present between the air-water interface and the cell substrate below. This allows us to more strongly control the size of this gap, increasing consistency between experiments and allowing for more rigorous testing of the effect depth has on the compressed

monolayer.

Confocal microscopy, an imaging technique used to produce three-dimensional imagery, could be of use for studying the physical dimensions of induced folds. This approach would allow us to directly image folds and determine their width and depth into the subphase in addition to the number of particles trapped within. This would provide information about the carrying-capacity that a typical fold can have for a particular size particle, thus more strongly highlighting their role in transport. In addition, by imaging the layer of cells, we should not only able to determine if material has been transported past the air-water interface, but also how readily the cells take up transported material into the cytoplasm.

Lastly, non-contact submerged microrheology, a technique developed by a previous graduate student in our lab, could be of use for studying this system. Here, a tracer particle is submerged at a fixed depth below the monolayer surface by a laser tweezer apparatus. The thermal fluctuations of this particle induce stresses and strains in the monolayer above and the resulting response function reveals information about physical properties of the monolayer and its collapse structures. It is of interest to determine if the fold structures have different properties than the adjacent in-plane monolayer. Measuring these properties could also help to understand the stability of folds and the conditions under which they can pinch-off or rupture.

Bibliography

[1] Wiliam Bialek, Andrea Canagna, Irene Giardina, Mora Thierry, Edmondo Silvestri, Massimiliano Viale, and Aleksandra M. Walczak. Statistical mechanics for natural flocks of birds. *PNAS (Proceedings of the National Academy of Sciences of the United States of America)*, 109(13):4786–4791, November 2012.

[2] Michael D. Manson, P.M. Tedesco, and Howard C. Berg. Energetics of flagellar rotation in bacteria. *Journal of Molecular Biology*, 138:541–561, April 1980.

[3] Q.D. Nguyen and D.V. Boger. Measuring the flow properties of yield stress fluids. *Annual Reviews Fluid Mechanics*, 24:47–88, 1992.

[4] Y. Jiang, P. Swart, A. Saxena, M. Asipauskas, and J. A. Glazier. Hysteresis and avalanches in two-dimensional foam rheology simulations. *Phys. Rev. E*, 59(5):5819–5832, May 1999.

[5] R. S. Ghaskadvi, J. B. Ketterson, and P. Dutta. Nonlinear shear response and anomalous pressure dependence of viscoity in a langmuir monolayer. *Langmuir*, 13(19):5137–5140, September 1997.

[6] T. G. Mason and D.A. Weitz. Linear viscoelasticity of colloidal hard sphere suspensions near the glass transition. *Phys. Rev. Lett.*, 75(14):2770–2773, Oct. 1995.

[7] S.L. Keller, H.E. Warriner, C.R. Safinya, and J. A. Zasadzinski. Direct observation of a defect-mediated viscoelastic transition in a hydrogel of lipid membranes and polymer lipids. *Phys. Rev. Lett.*, 78(25):4781–4784, Jun 1997.

[8] Robert Walder, Alex J. Levine, and Michael Dennin. Rheology of two-dimensional f-actin networks associated with a lipid interface. *Phys. Rev. E*, 77(1):5137–5140, Jan 2008.

[9] Patrycja Dynarowicz-Latka, Anatharaman Dhanabalan, and Osvaldo N. Olivera. Modern physiochemical research on langmuir monolayers. *Advances in Colloid and Interface Systems*, 91(2):221–293, 2001.

[10] Xia Qiu, Jaime Ruiz-Garcia, Keith J. Stine, Charles M. Knobler, and Johnathan V. Selinger. Direct observation of domain structure in condensed monolayer phases. *Phys. Rev. Lett.*, 67(6):703–706, Aug 1991.

[11] C. M. Knobler and R. C. Desi. Phase transitions in monolayers. *Annual Review of Physical Chemistry*, 43(1):207–236, 1992.

[12] Daniel K. Schwartz and Charles M. Knobler. Direct observations of transitions between condensed langmuir monolayer phases by polarized fluorescence microscopy. *The Journal of Physical Chemistry*, 97(35):8849–8851, September 1993.

[13] A. Saint-Jalmes, F. Graner, F. Gallet, and B. Houchmandzadeh. Buckling of a bidimensional solid. *EPL (Europhysics Letters)*, 28(8):565–571, 1994.

[14] Svetlana Baoukina, Luca Monticelli, H. Jelger Risselada, Siewert J. Marrink, and D. Peter Tieleman. The molecular mechanism of lipid monolayer collapse. *Proceedings of the National Academy of Sciences*, 105(31):10803–10808, August 2008.

[15] Christophe Ybert, Weixing Lu, Gunter Moller, and Charles M. Knobler. Collapse of a monolayer by three mechanisms. *The Journal of Physical Chemistry B*, 106(8):2004–2008, February 2002.

[16] Jonathan V. Selinger, Zhen-Gang Wang, Robijn F. Bruinsma, and Charles M. Knobler. Chiral symmetry breaking in langmuir monolayers and smectic films. *Physical Review Letters*, 70(8):1139–1142, November 1992.

[17] H Möhwald. Phospholipid and phospholipid-protein monolayers at the air/water interface. *Annual Review of Physical Chemistry*, 41(1):441–476, 1990.

[18] J. N. Hildebran, J. Goerke, and J. A. Clements. Pulmonary surface film stability and composition. *J. Appl. Physiol.*, 47(3):604–611, September 1979.

[19] S. Schürch. Surface tension at low lung volumes: dependence on time and alveolar size. *Respiration physiology*, 48(3):339–355, June 1982.

[20] W. Schief. Liquid-crystalline collapse of pulmonary surfactant monolayers. *Biophysical Journal*, 84(6):3792–3806, June 2003.

[21] J. Heyder, J. Gebhart, G. Rudolf, C. F. Schiller, and W. Stahlhofen. Deposition of particles in the human respiratory tract in the size range 0.005-15 /*mu*m. *Journal of Aerosol Science*, 17(5):811–825, 1986.

[22] H. Diamant, T. A. Witten, A. Gopal, and K. Y. C. Lee. Unstable topography of biphasic surfactant monolayers. *EPL (Europhysics Letters)*, 52(2):171–177, 2000.

[23] H. Diamant, T. A. Witten, C. Ege, A. Gopal, and K. Y. Lee. Topography and instability of monolayers near domain boundaries. *Phys. Rev. E*, 63(6), 2001.

[24] H. Diamant, T. A. Witten, K. Y. C. Lee, A. Gopal, and C. Ege. Topography and instability of model lung surfactant monolayers. *Biophysical Journal*, 82(1):547a–548a, 2002.

[25] T. A. Siebert and S. Rugonyi. Influence of liquid-layer thickness on pulmonary surfactant spreading and collapse. *Biophysical Journal*, 95(10):4549–4559, Aug 2008.

[26] P. Martin, M. Szablewski, and M. Keynes. *Tensiometers and Langmuir-Blodgett Troughs Operating Manual*, 4th edition, 1998.

[27] Alberta Iliff and Virginia A. Lee. Pulse rate, respiratory rate, and body temperature of children between two months and eighteen years of age. *Child Development*, 23(4):237–245, December 1952.

Appendix A

Source Code

A.1 Isotherm Isolation Program

Originally developed by Thomas Boatwright and modified by Chin-Chang Kuo.

```
function isotherm_process_v9(data_dir)
%% Picks out individual isothermal compressions and saves them.

files = dir(fullfile(data_dir,'surv*.txt'));

num_isotherm_sets = size(files, 1);

for k = 1:num_isotherm_sets

    [~, save_folder, ~, ~] = fileparts(files(k).name);

    save_dir = fullfile(data_dir, save_folder);
```

```
[~,~,~] = mkdir(save_dir);

imported = importdata(fullfile(data_dir,files(k).name),'\t');

Tinput = imported.data(:,1);

Ainput = imported.data(:,2);

Pinput = imported.data(:,6);


%% Try to find the transitions between comp and exp
Asmooth = smooth(Ainput,10);
dA = derivative(Asmooth);

expansions = find(dA > 0);
e = zeros(size(expansions));
e(1) = expansions(1) - 1;
e(2:end) = diff(expansions) - 1;
e = e(e~=0 & e>10);
e_mean = mean(e); % average number of points between expansions


compressions = find(dA < 0);
c = zeros(size(compressions));
c(1) = compressions(1) - 1;
c(2:end) = diff(compressions) - 1;
```

```
c = c(c~=0 & c>10);
c_mean = mean(c); % average number of points between compressions

%% identifies isotherm cycles

comp_numbers = zeros(size(Asmooth));
exp_numbers = zeros(size(Asmooth));
exp_rough = dA > 0;
isotherm_comp = 1;
isotherm_exp = 1;
for j = 2:length(Asmooth);
    if exp_rough(j) == 1 && exp_rough(j-1) == 1
        exp_numbers(j) = isotherm_exp;
    elseif exp_rough(j) == 0 && exp_rough(j-1) == 1
        comp_numbers(j) = isotherm_comp;
        isotherm_exp = isotherm_exp + 1;
    elseif exp_rough(j) == 1 && exp_rough(j-1) == 0
        exp_numbers(j) = isotherm_exp;
        isotherm_comp = isotherm_comp + 1;
    elseif exp_rough(j) == 0 && exp_rough(j-1) == 0
        comp_numbers(j) = isotherm_comp;
    else
    end



end
comp_numbers(1) = comp_numbers(2);
```

```
exp_numbers(1) = exp_numbers(2);

mean_buffer = 0.5; %50% of mean

for l = 1:max(comp_numbers)
    comp_check = find(comp_numbers == l);
    if length(comp_check) < mean_buffer*e_mean;
        comp_numbers(comp_check) = 0;
    end
end

for l = 1:max(exp_numbers)
    exp_check = find(exp_numbers == l);
    if length(exp_check) < mean_buffer*c_mean;
        exp_numbers(exp_check) = 0;
    end
end

comp_numbers = bwlabel(comp_numbers);
exp_numbers = bwlabel(exp_numbers);


num_compressions = max(comp_numbers);
num_expansions = max(exp_numbers);
compression_output_collection=cell(1,num_compressions);
expansion_output_collection=cell(1,num_expansions);
```

```
for j = 1:num_compressions
    T = Tinput(comp_numbers == j);
    A = Ainput(comp_numbers == j);
    P = Pinput(comp_numbers == j);
    K = -derivative(P)./derivative(A).*A;
    P_s = smooth(P,10);
    A_s = smooth(A,10);
    K_s = smooth(-derivative(P_s)./derivative(A_s).*A_s,10);
    compression_output = zeros(length(A),7);
    compression_output(:,1)=A;
    compression_output(:,2)=A_s;
    compression_output(:,3)=P;
    compression_output(:,4)=P_s;
    compression_output(:,5)=K;
    compression_output(:,6)=K_s;
    compression_output(:,7)=T;
    csvwrite(fullfile(save_dir,['isotherm compression '

     num2str(j)]),compression_output);
    compression_output_collection{j}=compression_output;
end

for j = 1:num_expansions
    T = Tinput(exp_numbers == j);
    A = Ainput(exp_numbers == j);
    P = Pinput(exp_numbers == j);
    K = -derivative(P)./derivative(A).*A;
```

```
        P_s = smooth(P,10);
        A_s = smooth(A,10);
        K_s = smooth(-derivative(P_s)./derivative(A_s).*A_s,10);

        expansion_output = zeros(length(A),7);
        expansion_output(:,1)=A;
        expansion_output(:,2)=A_s;
        expansion_output(:,3)=P;
        expansion_output(:,4)=P_s;
        expansion_output(:,5)=K;
        expansion_output(:,6)=K_s;
        expansion_output(:,7)=T;
        csvwrite(fullfile(save_dir,['isotherm expansion ' num2str(j)])

        ,expansion_output);
        expansion_output_collection{j}=expansion_output;
    end
%calcuation loop
        Mp_num=0;
        for i = 1:num_expansions;
            p_num = length(compression_output_collection{1,i}(:,1));
            if p_num >= Mp_num;
               Mp_num=p_num;
            end
        end
            A_P_cycles=NaN(Mp_num,num_expansions*4);
        for j = 1:num_expansions
```

```
A_P_cycles(1:length(compression_output_collection{1,j}
(:,1)),(j*4)-3)

=compression_output_collection{1,j}(:,1);
A_P_cycles(1:length(compression_output_collection{1,j}
(:,3)),(j*4)-2)

=compression_output_collection{1,j}(:,3);
A_P_cycles(1:length(expansion_output_collection{1,j}
(:,1)),(j*4)-1)

=expansion_output_collection{1,j}(:,1);
A_P_cycles(1:length(expansion_output_collection{1,j}
(:,3)),(j*4))

=expansion_output_collection{1,j}(:,3);

bin_P_A=isotherm_bin_average(
compression_output_collection

{1,j},0.5);
if  j==1;
     bin_P_A_cycles=zeros(length(bin_P_A(:,1)),num_expansions+1);
     bin_P_dm=zeros(length(bin_P_A(:,1)),num_expansions);
     bin_P_dm_to1=zeros(length(bin_P_A(:,1)),num_expansions);
     bin_P_A_cycles(:,1:2)=bin_P_A;
end
```

```
            bin_P_A_cycles(:,j+1)=bin_P_A(:,2);
            bin_P_dm(:,1)=bin_P_A_cycles(:,1);
            if j>=2;
                bin_P_dm(:,j)=1-(bin_P_A_cycles(:,j+1)
                ./bin_P_A_cycles(:,j));
            end
            bin_P_dm_to1(:,1)=bin_P_A_cycles(:,1);
            if j>=2;
                bin_P_dm_to1(:,j)=1-(bin_P_A_cycles(:,j+1).
                /bin_P_A_cycles(:,2));
            end
        end
    csvwrite(fullfile(save_dir,['A_P_cycles_compression']),A_P_cycles);
    csvwrite(fullfile(save_dir,['bin_P_A_cycles_compression']),
    bin_P_A_cycles);
    csvwrite(fullfile(save_dir,['bin_P_dm_compression']),bin_P_dm);
    csvwrite(fullfile(save_dir,['bin_P_dm_to1_compression']),
    bin_P_dm_to1);
end



end
```

A.2 Slope Analysis Program

```
SlopeAnalysis[data1_] := (
```

```
table1 =
 Table[{data1[[i]][[1]], data1[[i]][[3]]}, {i, 1, Length[data1]}];

SlopeData =
 Table[{Mean[{table1[[i]][[1]], table1[[i + 5]][[1]]}],
   table1[[i + 5]][[2]] - table1[[i]][[2]]}, {i, 1,
   Length[table1] - 5}];

cutoff = Select[SlopeData, #[[2]] >= 0.4 &];

DiffList =
 Table[Abs[cutoff[[i + 1]][[1]] - cutoff[[i]][[1]]], {i, 1,
   Length[cutoff] - 1}];

{Flatten[
   cutoff[[Flatten[Position[DiffList, Max[DiffList]]] - 1]][[1]],

 Max[DiffList]} )
```